IOP Publishing Journal of Physics B: Atomic, Molecular and Optical Physics
J. Phys. B: At. Mol. Opt. Phys. **47** (2014) 015201 (12pp) doi:10.1088/0953-4075/47/1/015201

Neonization method for stopping, mean excitation energy, straggling, and for total and differential ionization cross sections of CH_4, NH_3, H_2O and FH by impact of heavy projectiles

C C Montanari[1,2] **and J E Miraglia**[1,2]

[1] Instituto de Astronomía y Física del Espacio (CONICET-UBA), Casilla de correo 67, sucursal 28 (C1428EGA), Buenos Aires, Argentina
[2] Fac. de Ciencias Exactas y Naturales, Universidad de Buenos Aires, Buenos Aires, Argentina

E-mail: miraglia@iafe.uba.ar

Received 27 August 2013, revised 29 October 2013
Accepted for publication 14 November 2013
Published 11 December 2013

Abstract

We propose a *neonization* method to deal with molecules composed by hydrides of the second row of the periodic table of elements: CH_4, NH_3, OH_2 and FH. This method describes these ten-electron molecules as dressed atoms in a pseudo-spherical potential. We test it by covering most of the inelastic collisional magnitudes of experimental interest: ionization cross sections (total, single and double differential), stopping power, energy-loss straggling and mean excitation energy. To this end, the *neonization* method has been treated with different collisional formalisms, such as the continuum-distorted-wave–eikonal-initial-state, the first order Born, and the shell-wise local plasma approximations. We show that the present model reproduces the different empirical values with high reliability in the intermediate to high-energy region. We also include the expansion of the spherical wave functions in terms of Slater-type orbitals and the analytic expression for the spherical potentials. This makes it possible in the future to tackle present *neonization* strategy with other collisional models.

(Some figures may appear in colour only in the online journal)

1. Introduction

The theoretical description of inelastic collisions involving molecules at random and heavy projectiles is usually performed by first considering the molecule in a specific position and afterwards making an average of all the possible positions. By doing so, all the interference phenomena involving the different centres will be present. The angular and energy distributions of the emitted electrons will show the footprints of the geography of the partners conforming the molecule. However, by varying the position of the molecule at the end of the calculation, some of these patterns will be erased.

For simple molecules this method does not present major difficulties. But when the molecule is rather complex, the calculation becomes complicated, not due to the initial quantum mechanical states, which can be calculated with high precision [1], but because of the final continuum states, which are unknown. In many cases, it is necessary to resort to a combination of continuum states of the different atoms or ions in the molecule. In practice, Coulomb continuum states with effective charges are used. For example, the molecule of water, of clear biological interest, has been largely studied with this scheme [2–11], in ionization cross sections and also stopping power calculations.

The strategy we propose here is just the inverse: we first make an average of all possible positions of the molecule to

the point that we built a dressed atom in a pseudo-spherical potential, and then we perform the collisional calculation as an ion–atom collision. This procedure is much simpler and it has the important advantage that the initial as well as the final continuum states can be calculated exactly. But we have to pay a price: all the interferences among the different nuclei are buried.

This method can simplify and speed up numerous calculations involving hydrides, to which it applies quite well. Our goal is to substantiate this strategy as far as the total cross section, stopping power, straggling, and singly and even doubly differential cross sections are concerned. For any model, the decisive proof is the comparison with experiments, and this is what we are committed to in this work, testing the present method as thoroughly as we can.

Particularly, we will study ten-electron molecules: methane, CH_4, ammonia, NH_3, water, OH_2, and hydrogen fluoride, FH. We call this proposal the *neonization* method. *A priori* one would expect that CH_4, which has the maximum symmetry, is the more suitable to be treated with our one-centre spherical reduction. In contrast, the less favoured is the FH, which has a cylindric symmetry.

Among these four molecules, *water* is largely the most studied due to its application on biological studies. For water in its vapour phase there are several experimental measurements and tables of suggested values, ranging from total [12, 13], to singly [14] and doubly differential [15–17] ionization cross sections. Champion and collaborators have reported a series of detailed calculations of the total and differential ionization cross sections by the impact of heavy projectiles [5–11]. The energy loss of ions in water is another subject that has deserved special attention due to its application in tumour therapy. The experimental stopping power data available in the literature [18, 19] corresponds to solid, vapour and, recently, to liquid water too [20, 21], as reported in [18] and [22]. We will focus our comparison on the stopping power data of protons in vapour [23–26], but we will also compare it with the liquid and solid phase data at high energies. A sensitive quantity included in medicine simulations for proton treatment is the mean excitation energy [27–29]. This value is directly applied to get dose distributions and Bragg peak positions when high-energy projectiles penetrate matter. Differences around 15–20% have been noted among values of mean excitation energy of water suggested in the ICRU Reports [30, 31], the experimental data [32–36] and theoretical results [37–40], showing that a reliable value has not been established yet [27, 41, 42]. Another parameter of interest, also included in the depth–dose simulations, is the spread in the energy loss or energy-loss straggling, which introduces a limitation to determine the position and shape of the Bragg peak [29].

Methane has also been experimentally studied. Total, singly and doubly differential ionization cross sections were measured by Rudd, Toburen and collaborators [14, 43–48]. Specifically for hydrocarbons, in [47] a universal semi-empirical formula has been developed considering the number of weakly bound electrons. This formula is quite successful not only for hydrocarbon molecules, but also for the hydrides considered here. Several stopping power experiments have been compiled by Paul [18] and Ziegler [19] and are available online. A theoretical description of inelastic processes in this molecule has been performed using the continuum-distorted-wave–eikonal-initial-state (CDW–EIS) approximation with the molecular wave functions as linear combination of atomic ones [49, 50]. Also a theoretical method using Moccia initial states [1] and Coulomb continuum wave functions was reported in [51].

Less frequently, the literature includes measurements of ionization cross sections of *ammonia* [45, 46]. For stopping power, to our knowledge, the only experiments reported are those by Bourland *et al* [52, 53] considering He^{2+} impact. Unfortunately, on *hydrogen fluoride*, no experiments were found, and so we do not present any inelastic magnitude for this target. We recall that HF has axial symmetry, so is the less favoured by this spherical model.

In this contribution we present our theoretical results for the mentioned collisional parameters (i.e. total ionization cross sections, stopping power, energy-loss straggling, mean excitation energy, and single and double differential cross sections (DDCSs)) starting from two different sources. On one hand, we use the CDW–EIS approximation [54] and the first order Born approximation. These are binary collisional formalisms within the independent electron model. On the other hand, the dielectric formalism is employed by using the shell-wise local plasma approximation (SLPA) [55]. The SLPA describes the response of the electrons of the same binding energy as a whole (collectively, including all the electron interactions), screening the interaction with the impinging ion. This model considers separately each sub-shell of target electrons using the Levine–Louie dielectric response [56] to include the energy gap.

The *neonization* method we propose here for CH_4, NH_3, H_2O and HF can be applied to other Ne-type molecules of biological interest, such as OH^- and OH_3^+ [57], following exactly the same scheme. Thus, the *argonization* of the third row of the periodic table, the 18-electron molecules SiH_4, PH_3, SH_2, and ClH, would be a carbon copy of the developments proposed in the next section. In fact, one could also rise expectations, and attempt to *kriptonize* some molecules involving hydrides of Ge, As and Se, though taking into account that some of them are not stable.

This work is organized as follows. In section 2 the *neonization* method is described in detail, including the wave functions and binding energies obtained for the four molecules in terms of Slater-type orbitals. The results and the comparison with the experimental data is performed in section 3. Atomic units are used except when indicated.

2. The neonization method

Let us consider the following molecules: CH_4, NH_3, OH_2 and FH. The nuclear charge of the heavy elements are $Z_N =$ 6, 7, 8, and 9, and along with the number of hydrogens (4, 3, 2, and 1) all have ten electrons. Each molecule has N_H hydrogens localized at the positions $\mathbf{R}_H$, with $R = |\mathbf{R}_H|$ being a characteristic distance for each molecule.

The Hamiltonian of these targets is

$$H = -\sum_{i=1}^{10}\frac{1}{2}\nabla^2_{\mathbf{r}_i} - \sum_{i=1}^{10}\frac{Z_N}{r_i} + \sum_{i=1}^{10}V_H(r_i) + \sum_{j<i}^{10}\frac{1}{r_{ij}}, \quad (1)$$

where r_i is the position of the ith-electron with respect to the heavy nucleus, and V_H is the Coulomb potential originated by the $N_H = 10 - Z_N$ protons at $\mathbf{R}_H$, namely

$$V_H(\mathbf{r}) = -\sum_{\mathbf{R}_H}^{N_H}\frac{1}{|\mathbf{r}-\mathbf{R}_H|}. \quad (2)$$

Moccia [1] solved the equation $H\Psi_M = E\Psi_M$ by considering a one-centre expansion (OCE) method: $\Psi_M = R^{(M)}_{nl}(r)Y^m_l(\Omega)$ using Hartree–Fock where the radial functions where expressed in terms of Slater orbitals, $S_{nlm}(\varsigma|\, r,\theta,\phi)$, as follows

$$R^{(M)}_{nl}(r) = \sum_{\mu_j j} a^{(M)}_{\mu_j} S_{\mu_j}(\varsigma_j|\, r,\theta,\phi), \quad (3)$$

$$S_{\mu_j}(\varsigma_{\mu_j}|r) = \frac{(2\varsigma_{\mu_j})^{\mu_j+1/2}}{\sqrt{(2\mu_j)!}} r^{\mu_j-1}\mathrm{e}^{-\varsigma_{\mu_j}r}. \quad (4)$$

Moccia [1] obtained five states containing two electrons (spin up and down) on each orbit.

Our approximation is simpler. We consider that the N_H protons are part of a spherical surface of radius R where all of them are uniformly spread. From elemental electrostatics, we know that the potential is constant inside the sphere and Coulombic outside. Mathematically, we can cast this idea with the average

$$\langle V_H(\mathbf{r})\rangle = -\int\frac{\mathrm{d}\Omega_R}{4\pi}\sum_{\mathbf{R}_H}^{N_H}\frac{1}{|\mathbf{r}-\mathbf{R}_H|}, \\ = -\frac{N_H\Theta(R-r)}{R} - \frac{N_H\Theta(r-R)}{r}. \quad (5)$$

To some extent, this average anticipates the final random position of the molecule. The reader from the atomic physics community will recognize this approximation as an extension of the Temkin–Poet model [58], originally designed to treat helium. We approximate $V_H(\mathbf{r})$ by the central potential

$$V_H(r) \simeq -\frac{N_H(1-\varepsilon)\Theta(R-r)}{R} \\ -\frac{N_H(1-\varepsilon\,\mathrm{e}^{-r/R})\Theta(r-R)}{r}, \quad (6)$$

where we have introduced one defect, ε , to correct the failure of our spherical hypothesis (more precisely, to adjust the energies). We display in table 1 the values of ε used. We will return to this point later, in relation to the curves displayed in figure 1.

The Hamiltonian in (1) is then approximated by a dressed atom Hamiltonian H_C

$$H \simeq H_C = -\sum_{i=1}^{10}\frac{1}{2}\nabla^2_{\mathbf{r}_i} - \sum_{i=1}^{10}V_C(r_i) + \sum_{j<i}^{10}\frac{1}{r_{ij}}, \quad (7)$$

with

$$V_C = -\frac{Z_C(r)}{r}, \quad (8)$$

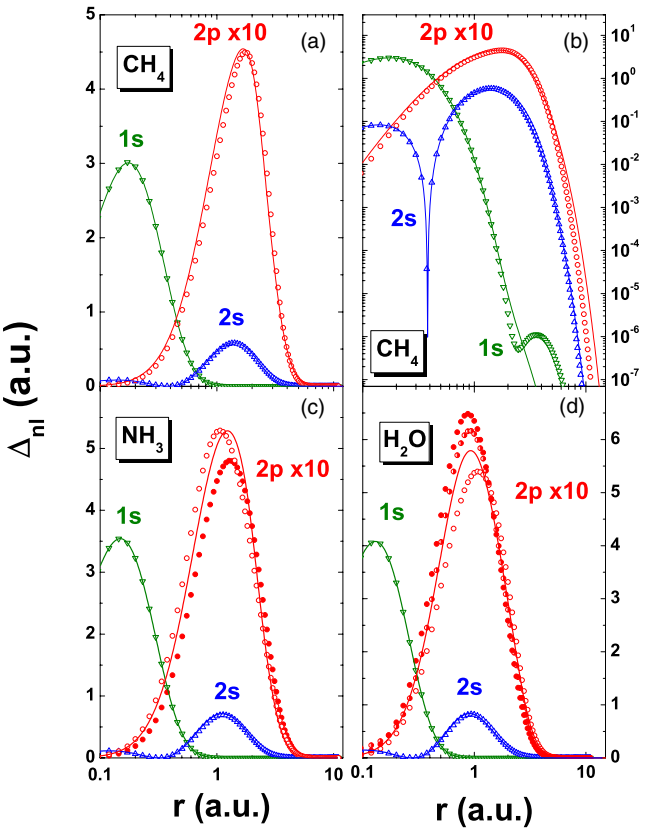

Figure 1. Comparison between spherical electron densities given by (12). Solid lines, present densities; symbols, Moccia OCE molecular densities [1]. Figures (a), (c) and (d) for CH_4, NH_3 and OH_2, respectively. Figure (b), the same as (a) in logarithmic scale.

Table 1. Characterization of the molecules in the dressed atom central approximation. The values R (distance of the hydrogen atoms to the heavy centre element) and ε are parameters included in (9); E_{nl} and r_{nl} are the obtained binding energies and mean radii of the nl-states, respectively; E_t, E_k, E_x and E_c are the total, kinetic, exchange and correlation energies, respectively. The ratios α and β are defined in (11). Atomic units are used.

		CH_4	NH_3	OH_2	FH
Parameters					
	R	2.080	1.928	1.814	1.728
	ε	−0.0975	−0.103	−0.325	−0.085
Hartree–Fock					
	E_{1s}	−11.11	−15.45	−20.56	−26.25
	E_{2s}	−0.954	−1.124	−1.300	−1.576
	E_{2p}	−0.502	−0.542	−0.584	−0.678
	r_{1s}	0.269	0.229	0.199	0.176
	r_{2s}	1.694	1.423	1.229	1.032
	r_{2p}	1.913	1.634	1.468	1.163
	E_t	−54.28	−68.84	−84.63	−105.5
	E_k	39.97	56.21	75.36	100.1
	E_x	−6.629	−7.827	−8.963	10.65
	E_c	−0.208	−0.238	−0.266	−0.308
Ratios					
	$\alpha_k^{(\mathrm{LPA})}$	1.100	1.099	1.098	1.094
	$\beta_x^{(\mathrm{LPA})}$	1.107	1.106	1.119	1.117
	$\alpha_k^{(\mathrm{LLP})}$	1.093	1.095	1.098	1.095
	$\beta_x^{(\mathrm{B})}$	1.130	1.125	1.106	1.102

$$Z_C(r) = Z_N + N_H(1-\varepsilon)\frac{r}{R}\Theta(R-r) + N_H(1-\varepsilon\,\mathrm{e}^{-r/R})\Theta(r-R). \quad (9)$$

Note that

$$Z_C(r) \to \begin{cases} Z_N, & as\ \ r \to 0, \\ 10, & as\ \ r \to \infty, \end{cases} \quad (10)$$

which are the correct nuclear Coulomb limits.

We then proceed to do a full Hartree–Fock calculation, $H_C\Psi_C = E_C\Psi_C$, using the NRHF code by Johnson [59]. We adapted this code in order to incorporate the central charge $Z_C(r)$ instead of the punctual Z_N one. As $V_C(r)$ is a central potential, the solution can be expressed as: $\Psi_{Cnlm}(r) = R^{(C)}_{nl}(r)Y^m_l(\Omega)$, with nl = 1s,2s, and 2p. Eigenenergies (E_{nl}), mean values (r_{nl}), total energies (E_t), exchange (E_x), and kinetics (E_k) energies are displayed in table 1 for CH_4, NH_3, H_2O and FH, within the dressed atom picture. Correlation is not accounted for by Hartree–Fock method. Just to fulfil a detailed description of these dressed atoms, we have also calculated the correlation energies, (E_c), with the Wigner–Clementi expression [60][3]. All of these values hold on their own in their context, and should not be literally confronted with a full molecular calculation since our approximation avoids the electron concentration around the hydrogen atoms. It is important to note that in this case the Virial theorem does *not* hold, and this is because V_C is nonCoulombic (the Virial theorem for the Coulomb potential states that $E_k = -E_t$).

These E_{2p} energies can be compared with the experimental ionization potentials (IP) of each molecule. For CH_4 our theoretical value $|E_{2p}| = 13.6$ eV is lower but close to the experimental IP, 14.4 eV [61]. For NH_3, H_2O and FH we obtained $|E_{2p}| = 14.7$ 15.9 and 18.5 eV, respectively; all of them higher than the experimental IPs 10.1, 12.6 and 16.0 eV [61]. We will return to this later in this work in relation to our results for the ionization cross sections.

As for any atom, we can also calculate the exchange and kinetic energy in the local density approximation (LDA) [62], and the gradient correction given by Becke (B) [63] and Lee, Lee and Parr (LLP) [64] approximations. In table 1 we also displayed the corresponding ratios

$$\alpha^{\mathrm{LDA}} = E_k/E_k^{\mathrm{LDA}}, \quad \beta^{\mathrm{LDA}} = E_x/E_x^{\mathrm{LDA}}, \quad \alpha^{\mathrm{LLP}} = E_k/E_k^{\mathrm{LLP}}, \quad \beta^{\mathrm{B}} = E_x/E_x^{\mathrm{B}}. \quad (11)$$

These values are quite expectable and ratify the generalized suspicion that $\alpha \simeq \beta$.

In figure 1 we plot the local densities obtained from the present calculation with a central potential (Ψ_C), and from the average value of Moccia wave functions (Ψ_M), given by

$$\Delta_{C|M}(r) = r^2 \int \mathrm{d}\Omega\ \Psi^*_{C|M}\Psi_{C|M}. \quad (12)$$

These densities satisfy the normalization condition: $\int \mathrm{d}r\,\Delta_{C|M}(r) = 1$. As can be observed in figure 1, our averaged densities Δ_C for CH_4, NH_3, H_2O compares quite well with the ones of Moccia Δ_M in the region of interest. We must note that the Moccia states are five [1], so the outer three states should be compared with our 2p-state. In fact, we have chosen the values of ε displayed in table 1 so that the energy of our 2p-state approximates the average of the outer states obtained by Moccia [1]. Other criteria can be essayed, but it is pertinent to mention that even considering $\varepsilon = 0$, the final results do not change considerably.

As we can see for CH_4 in figure 1(b) in logarithmic scale, our densities do not match the ones by Moccia at large distances. We cannot describe the clear structure of the 1s-state at the protons' site. It could be reproduced by choosing a more elaborated central potential, for example one of the types used in [51]. As expected, similar features are found for NH_3 and H_2O, but are much less pronounced.

We performed a fitting of our wave functions Ψ_C with six Slater orbitals S_μ

$$R^{(C)}_{nl}(r) = \Sigma_{\mu_j} a_{\mu_j} S_{\mu_j}(\varsigma_{\mu_j}|r). \quad (13)$$

The coefficients of these Slater orbitals are displayed in table 2 for CH_4, NH_3 and H_2O. We want to stress that we forced the last charge value of the p-state to be $\varsigma_{\mu_6} = \sqrt{2|E_{2p}|}$, in order to properly describe the atomic density at large distances.

The values displayed in tables 1 and 2 are the only inputs for SLPA calculations [55] of ionization cross sections, stopping power or any other moment of the energy loss. Once the binding energies and the electronic densities are known, we can use the SLPA in the usual way [65–68].

Instead, if we are interested in the calculation based on the independent electron model, such as the first Born approximation or a distorted wave, such as the CDW–EIS, we need to specify the central potential for each electronic state. Namely, we have to determine $V_{nl}(r)$, so that

$$\left(-\frac{1}{2}\frac{\mathrm{d}^2}{\mathrm{d}r^2} + V_{nl}(r) + \frac{l(l+1)}{2r^2} - E_{nl}\right) u^C_{nl}(r) = 0, \quad (14)$$

where $R^C_{nl}(r) = u^C_{nl}(r)/r$. It is convenient to cast $V_{nl}(r)$ in terms of the popular form

$$V_{nl}(r) = -\frac{1}{r} - \sum_{j=1}^{2}\frac{Z_j}{r}(1+\alpha_j r)\,\mathrm{e}^{-\mu_j r}. \quad (15)$$

To obtain these parameters, we first determined a static form of $V_{nl}(r)$ knowing the density. Afterward, we polished it by imposing that the potential satisfies the correct binding energy E_{nl}, the mean values r^{-1}_{nl} and r_{nl}, as given in table 1. A set of values Z_j, μ_j and α_j for the four different molecules are displayed in table 3. Note that, in all cases, $V_{nl}(r)$ presents the correct limits, i.e. $V_{nl}(r) \to Z_N(1)$ as $r \to 0\ (\infty)$.

The independent electron model (CDW–EIS or Born approximations) only requires the potential $V_{nl}(r)$. It considers only the interaction of the projectile with a single electron while all the other electrons remain frozen. The wave functions for the bound and the continuous states are calculated by solving the Schrödinger equation of a single electron in this potential. The use of $V_{nl}(r)$ automatically determines all of the single-electron energy spectrum. In this regard, the first excited state for the four cases studied corresponds to the 3s state. Using the Salvat *et al* computing code [69] with V_{2p}, we obtained $E_{3s} = -0.234$, -0.194 and -0.181 au, for CH_4, NH_3

[3] (The density correlation energy is refitted as $\epsilon_c = \epsilon_{c1}\delta^{4/3}/(\epsilon_{c2}+\delta^{1/3})$, δ is the density and $\epsilon_{c1} = -0.189$ and $\epsilon_{c2} = 5.80$. This expression improves the Wigner one).

Table 2. Parameters defining the Slater orbitals, as given by (13).

	$CH_4(2p)$			$CH_4(2s)$			$CH_4(1s)$	
μ	ς_μ	a_μ	μ	ς_μ	a_μ	μ	ς_μ	a_μ
2	2.539 15	1.554 44	1	1.934 01	−13.5010	1	5.786 19	0.602 3296
2	10.1794	0.000 855	1	11.5329	0.005 39	1	9.702 84	0.055 044
2	2.210 01	−3.038 85	1	3.205 87	6.740 05	1	4.907 50	0.347 142
2	1.088 64	0.526 79	2	2.504 68	6.950 11	2	3.490 19	0.004 208
2	1.833 94	1.977 83	2	1.711 39	0.778 07	2	2.176 12	0.002 859
2	1.004 50	0.017 67	2	1.417 74	−0.698 08	2	1.390 23	0.000 539
	$NH_3(2p)$			$NH_3(2s)$			$NH_3(1s)$	
μ	ς_μ	a_μ	μ	ς_μ	a_μ	μ	ς_μ	a_μ
2	2.872 33	2.806 04	1	2.094 73	−3.807 28	1	6.958 63	0.546 789
2	10.6384	0.001 64	1	12.0911	0.008 484	1	11.5764	0.041 831
2	2.594 96	−5.579 76	1	4.097 35	1.771 51	1	5.846 72	0.415 018
2	1.253 79	0.472 56	2	2.859 18	2.082 41	2	4.148 03	0.004 600
2	2.306 23	3.292 09	2	1.717 66	−0.318 03	2	2.508 93	0.002 358
2	1.041 65	0.073 10	2	1.432 58	−0.199 67	2	1.545 46	0.000 413
	$OH_2(2p)$			$OH_2(2s)$			$OH_2(1s)$	
μ	ς_μ	a_μ	μ	ς_μ	a_μ	μ	ς_μ	a_μ
2	5.198 61	0.999 80	1	5.8539	0.530 52	1	7.857 50	0.739 34
2	7.862 57	0.029 77	1	7.5205	−0.264 25	1	13.5304	0.033 21
2	1.282 59	0.349 73	1	9.7902	0.082 27	1	6.226 86	0.233 82
2	1.948 50	0.519 06	2	4.5317	−0.233 45	2	3.236 05	0.002 49
2	5.442 18	−0.858 72	2	2.1371	−0.759 58	2	2.229 58	0.000 46
2	1.076 40	0.051 77	2	1.5464	−0.184 36	2	1.631 95	0.000 25

Table 3. Parameters defining the central potentials as given by (15).

State	j	Z_j	μ_j	α_j
$CH_4(2p)$	1	−1.0684	0.1183	−0.003 17
	2	−3.9316	3.0610	−0.073 78
$CH_4(2s)$	1	−1.3163	0.1189	0.055 66
	2	−3.6837	3.3510	−0.370 47
$CH_4(1s)$	1	−2.8922	0.5878	−0.042 53
	2	−2.1078	3.7098	0.047 48
$NH_3(2p)$	1	−1.5688	0.4003	0.000 00
	2	−4.4312	3.1936	−0.083 80
$NH_3(2s)$	1	−1.2827	0.1289	0.030 35
	2	−4.7173	2.8893	−0.214 71
$NH_3(1s)$	1	−1.1368	5.8363	−0.048 25
	2	−4.8632	1.1651	−0.019 03
$OH_2(2p)$	1	−1.9107	0.6499	−0.006 60
	2	−5.0893	3.2101	0.003 29
$OH_2(2s)$	1	−1.1543	0.1370	0.003 69
	2	−5.8457	2.8042	−0.029 80
$OH_2(1s)$	1	−0.9924	6.9585	−0.029 41
	2	−6.0076	1.4148	0.000 00

and H_2O, respectively. This gives theoretical first electronic excitation energies $\omega_g = E_{3s} - E_{2p} = 7.4$, 9.5 and 11.0 eV for these molecules, while the experimental (molecular) values are 10.9, 5.7 and 7.1 eV, respectively [61]. This first excitation energy gap is important when we consider stopping power, as we shall see later on in this contribution.

2.1. Numerical details

The starting element for the CDW–EIS model is the T-matrix element given by $T^{\mathrm{CDW-EIS}} = \langle \Psi^{\mathrm{CDW}-}|H - E|\Psi^{\mathrm{EI}+}\rangle$, where $\Psi^{\mathrm{CDW}-}$ ($\Psi^{\mathrm{EI}+}$) is the final (initial) distorted state [54]. The CDW final state $\Psi^{\mathrm{CDW}-}$ is written as the final continuum state times the projectile distortion, while the initial $\Psi^{\mathrm{EI}+}$ as the initial electronic state times the projectile eikonal distortion. The point we stress here is that the initial as well as the final continuum states are numerical (exact) solutions of the dressed atom considered. To that end, we used the code RADIALF [69] in a grid of about 2000 points of each of the 28 angular momenta of the continuum state. Further, we used 28 azimuth and polar angles of the ejected electrons, about 50 momentum transfers and 50 electron energies. Numerical integrations were carried out in these grids with the cubic spline technique. With the stopping power in mind, we have extended the CDW–EIS for excitation as well, which involves the numerical solution of the Schrödinger equation for the initial and final excited state in the same potential V_{nl} (see appendix of [70] for details of the algebra involved). Transitions to 3s, 3p, 3d, 4s, 4p and 4d, including all the magnetic sub-states, were calculated.

We also calculated the Born approximation in the same way. This is of particular importance, since the first order Born provides the correct high-energy limit.

On the other hand, we also employed the dielectric formalism through the SLPA. It is a first order method (Z_P^2 dependence), which works within the independent shell approximation [55]. The SLPA considers separately each nl-subshell and the interaction with an electron embedded in a fully correlated electron cloud. The high-energy limit should be given by both the first Born approximation and the SLPA (first order both), which lets us check them against each other.

The energy gap, ω_g, is introduced in the SLPA by using the Levine–Louie dielectric function [56], which includes it explicitly [55]. If we calculate ionization cross sections, the gap is the energy threshold of the state to be ionized, namely $\omega_g = |E_{nl}|$. But when we calculate the electronic energy loss or stopping power, all the inelastic processes are involved, including excitation too. In this case we used Levine–Louie dielectric function with an energy gap $\omega_g = E_{3s} - E_{nl}$, where

E_{nl} corresponds to the initial state, and E_{3s} is the energy of the first excited state given before. In all cases, this dielectric function satisfies the *f-sum* rule, which ensures the correct behaviour of the SLPA at high energies and the tendency towards the Bethe limit [71]. We will return to this point again in relation to the mean excitation energy.

3. Results

Our starting points are condensed in tables 1–3, no other data is required. For the CDW–EIS we only need the potentials given by (15) and the coefficients of table 3, energy, initial bound and final continuum states were obtained solving the Schrödinger equation numerically. For the SLPA calculations we require the densities of each sub-shell of electrons (obtained from the wave functions given in table 2) and the corresponding binding energies (given in table 1).

3.1. Total cross section

Figure 2 shows the total ionization cross sections of CH_4, NH_3, and OH_2 by proton impact. Our three theories are displayed: Born approximation in dotted lines, the CDW–EIS in solid lines and the SLPA in dash-dotted lines. We will keep this representation all throughout this work.

As expected, the CDW–EIS values tend to the Born approximation for high proton energies (impact energy $E >$ 300 keV). We performed CDW–EIS calculations for proton impact energies up to 1 MeV and tested this convergence. There is no need to employ the CDW–EIS approximation for higher energies because the Born approximation provides the results with much less computing time (about one order of magnitude less). At lower energies the behaviour is the usual one: the Born approximation becomes larger and CDW–EIS diminishes. In all the cases the high-energy limit falls on the experiments which is a guaranty that our model works quite well. It should be noted that the SLPA provides the high-energy limit quite precisely and this is good news, since this simple model is computationally very fast, much faster than the Born approximation. In fact, we first calculate with the SLPA and inspect the ranges of all the variables of interest where the process is relevant.

Total experimental cross sections are also displayed in figure 2, together with the recommended values by Rudd *et al* in [44]. In the case of NH_3, few measurements are available, only those by Lynch *et al* [45] for $E \geqslant 250$ keV and by McNeal [46] for $E \leqslant 30$ keV. The recommended values by Rudd *et al* [44] extrapolate them proposing certain fitting function. On the other hand, for H_2O, in the last 20 years it has become possible to measure proton impact ionization cross sections leading to different dissociative and non-dissociative channels [72–74] (H_2O^+, OH^+, O^+, O^{2+}, H^+). The addition of these values is in good agreement with the total ionization cross sections by Rudd *et al* [12]. As an example, in figure 2 we include the total values for pure ionization obtained by adding the different contributions by Luna *et al* [74], for energies above 500 keV. We also include in figure 2 the high-energy data of electron impact ionization by Rao *et al* [75] (for NH_3) and by Itigawa *et al* [76] (for H_2O).

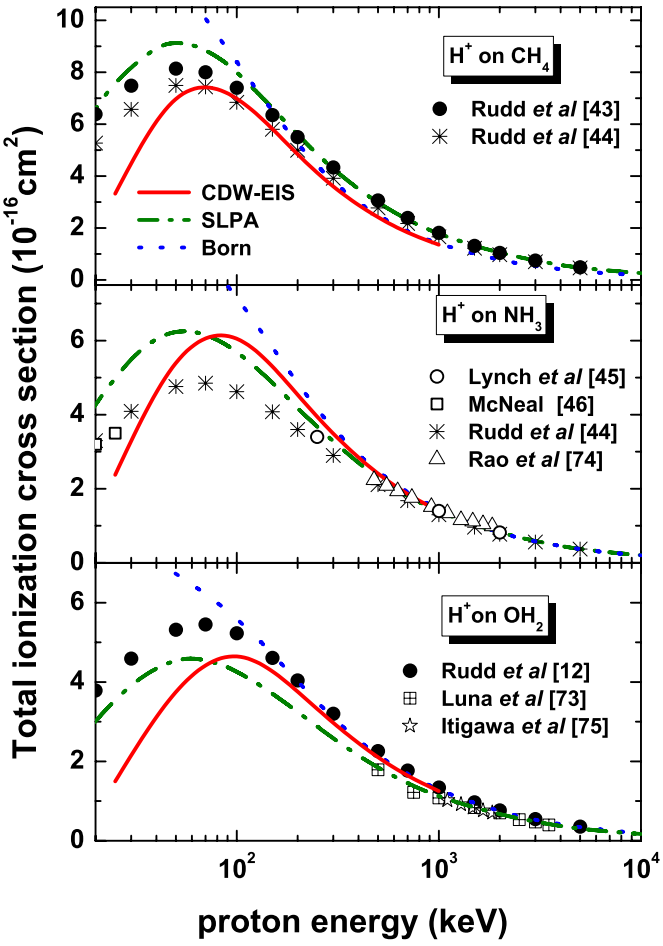

Figure 2. Total ionization cross section for protons on CH_4, NH_3 and H_2O, as a function of the impact energy. Curves: our theoretical results using the following approximations: solid lines (red) CDW–EIS, dotted lines (blue) first Born, and dashed–dotted lines (green) SLPA. Symbols: for CH_4, experimental data by Rudd *et al* [43] and recommended values (fitted) by Rudd *et al* [44]; for NH_3, experimental data by Lunch *et al* [45] and by McNeal [46], recommended values by Rudd *et al* [44], and data by Rao *et al* [75] for high-energy electron impact; for H_2O, experimental data by Rudd *et al* [12] and by Luna *et al* [74] for proton impact; also data by Itigawa *et al* [76] for high-energy electron impact.

As expected, the best agreement of the *neonization* model is found for methane, due to the high symmetry of this almost spherical molecule. The worst description seems to be for ammonia. However, the lack of measurements around the maximum of the cross section renders this inconclusive. For water vapour the agreement of the CDW–EIS is rather good for energies above 200 keV. These total ionization cross sections are in good agreement with CTMC calculations by Errea *et al* [77] and with CDW–EIS calculations by Champion *et al* [5].

The SLPA results are very sensitive to the energy gap introduced in the Levine–Louie dielectric function. Our theoretical outermost binding energy $|E_{2p}|$ is similar but lower than the known experimental value for CH_4 [61]. This may explain the small overestimation of the ionization cross section for this target. In contrast, for water our theoretical $|E_{2p}| = 15.9$ eV is somewhat larger than the experimental value and our SLPA underestimates the data. In fact, if we run the SLPA code changing only our theoretical $|E_{2p}|$ by the

experimental IP of water, 12.6 eV [61], or by the energy of Moccia outer molecular orbital 13.5 eV [1], the agreement of the SLPA with the experimental data is quite good in almost the whole energy range.

We have also calculated the total ionization cross section of water by impact of 6 MeV/amu C^{6+}, by using both, the first Born and the CDW–EIS approximations. We obtained values around 1×10^{-15} cm^2 in agreement with the results by Champion *et al* [8], but larger than the experiment situated at 5×10^{-16} cm^2 (see figure 3 in [8]).

3.2. Single differential cross sections

A deeper test of our model is to calculate the single differential cross section, $\mathrm{d}\sigma/\mathrm{d}E_e$, in terms of the emitted electron energy E_e. This magnitude samples different regions: from glancing (small-energy region) to head on (high-energy) collisions. It is known that $\mathrm{d}\sigma/\mathrm{d}E_e$ falls down several orders of magnitudes in terms of E_e. Instead the Platzman yield Y defined as

$$Y = \frac{\mathrm{d}\sigma}{\mathrm{d}E_e} \frac{v^2}{2\pi\,(E_e + |E_{2p}|)^2} \tag{16}$$

provides a much more detailed magnitude to inspect. For large values of v, the Platzman yield Y comes near to the number of active electrons, and for electron energies larger than the maximum energy transfer to a stationary electron, i.e. $E_e > (2v)^2$, Y decreases dramatically. Figure 3 shows the experimental Y values by Rudd and collaborators [14], for ionization of CH_4 and OH_2 by proton impact, along with our theoretical values obtained with CDW–EIS and the first Born approximation. Again, the CDW–EIS results for CH_4 are in very good agreement with the data in the whole spectrum of emitted electron energies, even for rather low impact energy. Of course, the agreement with Born decreases with decreasing impact energies. For water, the Platzman yields agree rather well with the experiments, except for the lower energies of the emitted electrons (i.e. $E_e < 10$ eV)

3.3. Double differential cross sections

A more thorough test of our model is the calculation of the DDCS in terms of the emitted energy and angle, i.e. $\mathrm{d}^2\sigma/\mathrm{d}E_e\mathrm{d}\Omega$. To describe the details, such as the capture to the continuum peak, we should resort to the CDW–EIS. Such a peak is absent in the first Born approximation.

The left and central panels of figure 4 show the CDW–EIS DDCS of protons on CH_4 and H_2O. The agreement is good, except at small angles and electron energies; this is a pathological failure of the CDW–EIS and not a fault of our *neonization* method.

In the right panel of figure 4 we change the view and display the DDCS for protons on NH_3 at an emitted electron angle of 125°. It is well known that emissions at backward angles are very sensitive to the quality of the continuum state, a simple Coulomb continuum with an effective charge generally fails. Our approximation provides a good description of the experiments along four orders of magnitude of the falls, which guarantees the quality of our continuum final state. The peak observed for NH_3 in figure 4, for emitted electrons around 300 eV, corresponds to the Auger decay. If we inspect the

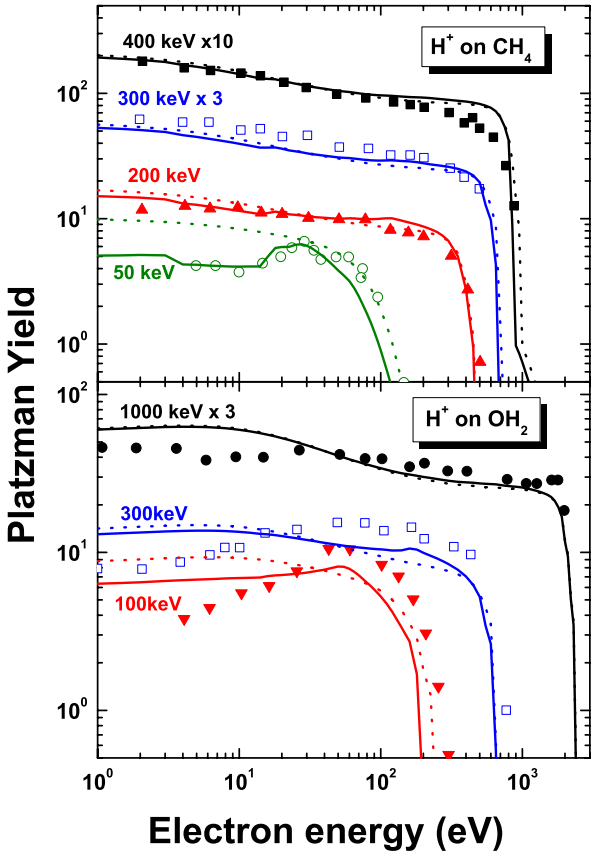

Figure 3. Platzman yields as a function of electron energy, given by (16) for different values of the proton impact energy as indicated. Upper and lower panels, results for CH_4 and OH_2, respectively. Experiments from [14]. Theoretical calculations are denoted by curves: solid lines, CDW–EIS; dotted lines, first Born approximation.

right panel in detail, it is evident that the theory overestimates slightly the experiments in the range between 1 and 10 eV. This tendency may explain the overestimation of the experimental data of the total ionization cross section for the ammonia target in figure 2.

3.4. Stopping power

The electronic stopping power is the energy loss by the projectile in all the possible inelastic processes, i.e. ionization, excitation, capture. In our CDW–EIS and first Born calculations for the stopping cross section, we include ionization and excitation to $n = 3$ and 4. For the SLPA values, we include ionization and excitation by considering transitions above the first possible excited state. This was done by using the Levine–Louie dielectric function with an energy gap $\omega_g = E_{nl} - E_{3s}$, as mentioned before. The capture contribution to the energy loss is not included in present calculations.

In figure 5 we display the results with our three theories, together with the experiments available in the literature [18, 19]. As a general behaviour, above 200 keV the three theories agree and nicely describe the experimental values.

In the upper figure, for CH_4, the data compiled by Paul [18] is included. We obtained a very good description of the

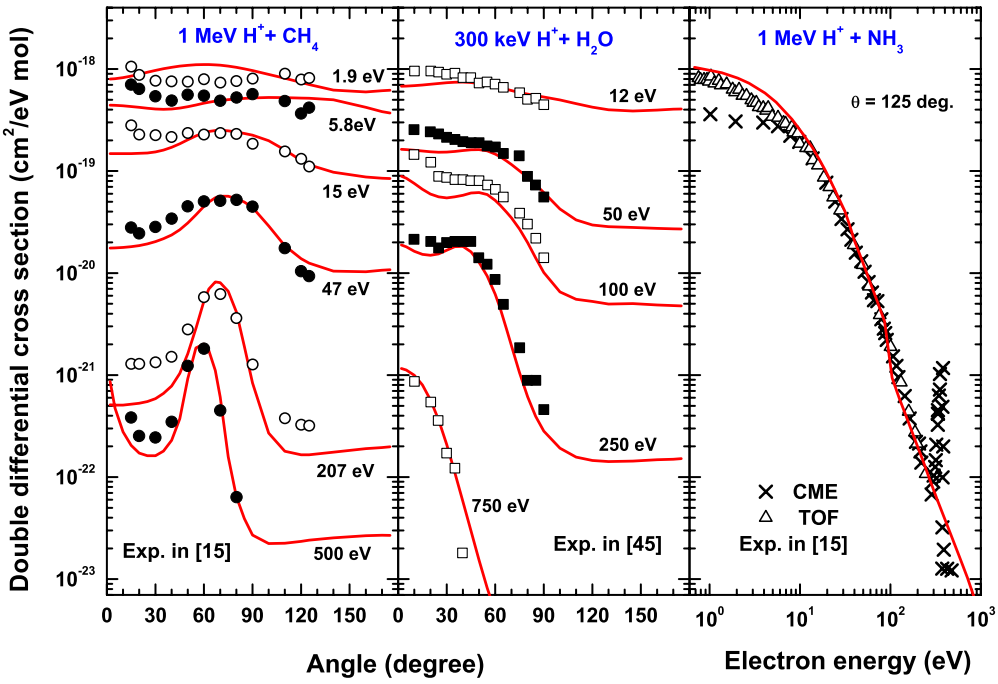

Figure 4. DDCS for the impact of protons on CH_4 at 1 MeV, on OH_2 at 300 keV, and on NH_3 at 1 MeV. Left and central panels, differential distribution as function of the ejection angles for different electron energies, as indicated. Right panel, differential distribution as a function of the emitted electron energy for a 125° ejection angle. Curves: solid lines, CDW–EIS results. Symbols: experimental data by Toburen *et al* [15] for CH_4 and NH_3, and by Lynch *et al* [45] for OH_2.

stopping maximum by using the SLPA. Also the CDW–EIS values describe the experiments above 100 keV. Below this energy capture cross section is not negligible [43] and should be considered to describe the experimental data.

For NH_3 the only measurements we found in the literature correspond to the impact of He^{2+} by Bourland *et al* [52, 53]. We found a reasonable agreement with the CDW–EIS in this target at the maximum of the stopping and a very good description at high impact energies. The use of the CDW–EIS here is mandatory since this projectile requires higher orders in the projectile charge, not included in the other two theories (Born and SLPA), which clearly overestimate the data.

In the lower plot of figure 5 we display the theoretical and experimental values for water vapour. Due to the importance of this target, a vast compilation of data is available [18], for the vapour, liquid or solid phases. We include in figure 5 experimental data for vapour, but also for ice and liquid water in the high-energy range (above 200 keV), where all the phase effects seem to disappear. This lets us extend the comparison due to recent measurements of the stopping of protons in liquid water above 4 MeV [21]. In the high-energy region, we also include the stopping data of He^{2+} in vapour, normalized to the square of the ion charge [18]. The agreement of this value with those of protons in vapour is very good and extends the energy range up to 2 MeV. On the other hand, the data for stopping in liquid water by Shimizu *et al* [20] is 10% below the experimental and theoretical values for vapour. This difference has already been noted [22, 79]. Below 200 keV, our results underestimate the experimental stopping of protons in water vapour. We attribute this to the lack of capture in our results. Around 50 keV the capture cross section of proton in vapour is similar to the ionization one [80, 81]. The importance of this contribution to the stopping power for proton impact energy below 100 keV has already been shown [82, 83].

3.5. Mean excitation energy

The mean excitation energy of compounds has been theoretically studied (compounds versus mixtures using Bragg's rule) a long time ago [84]. At high but not relativistic energies this value is related to the stopping power by the Bethe formula [71]

$$L(v) = \ln\left(\frac{2v^2}{I}\right), \tag{17}$$

where $L(v)$ is the stopping number, a dimensionless parameter defined as

$$L(v) = \frac{v^2}{4\pi Z_p^2 Z_T} S(v), \tag{18}$$

with $S(v)$ being the stopping cross section.

In this work we extend the test of the *neonization* model to the mean excitation energy I for each molecular target. In figure 6 we display our SLPA, CDW–EIS and first Born values for the stopping number of gaseous methane, ammonia and water. In the three cases, the SLPA tends to a straight line at high energies (a logarithmic dependence with v^2), as already noted for other targets (Au, Pb, Bi and W in [67]), showing that this model is tied to Bethe limit at high energies. The tendency to follow a straight line for energies above 500 keV amu^{-1} is also clear in the experimental data of CH_4 and H_2O. For NH_3 there are no measurements at high energies, and would be an interesting experimental–theoretical test to carry out.

It can also be noted in figure 6 that our first Born results deviate from the Bethe limit (and from the experimental data)

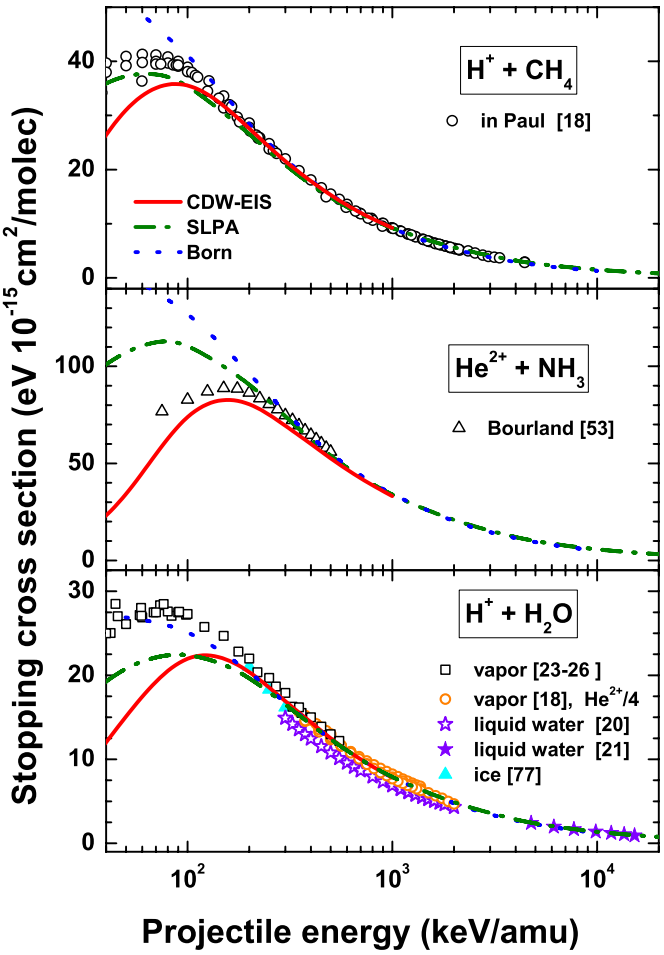

Figure 5. Stopping power cross section for the impact of protons on CH_4 and OH_2, and He^{2+} on NH_3. The theoretical calculations are denoted by lines. Solid lines (red) CDW–EIS, dotted lines (blue) Born approximations, and dotted-dashed lines (green) the SLPA approximation. Experimental data: for CH_4, Paul compilation [18]; for NH_3, measurements by Boulard *et al* [53] for He^{2+} impact; for H_2O, hollow squares correspond to water vapour [23–26], solid triangles to ice [78], hollow [20]and solid [21] stars to liquid water. We also include hollow circles (orange) for the stopping cross section of vapour for He^{2+}. [18]

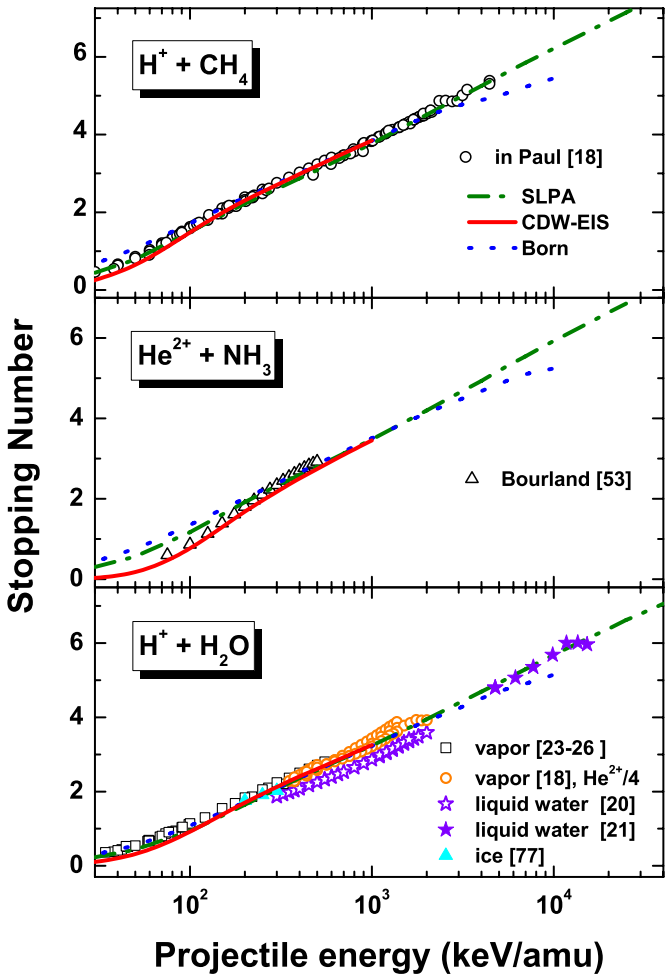

Figure 6. Stopping number as function of the impact energy, for the impact of protons on CH_4 and H_2O, and He^{2+} on NH_3. Notation for curves (theoretical results) and symbols (experimental data) as in figure 5.

for high energies (i.e. above 2 MeV). This is related to the number of angular momentum considered. We used just 24 angular momenta of the continuum state, and it is not enough to represent very high-energy electrons that contribute most to the stopping number at high impact energies.

The stopping number of H^+ on water enhances the behaviour already noted of the recent measurements of stopping in liquid water [20]. While the values by Siiskonen *et al* [21] above 4 MeV clearly follow the straight line, the values by Shimizu *et al* [20] are comparatively low.

The use of the mean excitation energy of water, I_{H_2O}, in dose distributions in hadron therapy, has triggered different theoretical and experimental efforts to reach a reliable value. Reviews of the *state of the art*, including suggested, measured and calculated values can be found in [79] and [27].

We use the SLPA results for the stopping number at high energies to obtain the mean excitation energy $I^{\rm SLPA} = \lim_{v\to\infty} 2v^2\, e^{-L(v)}$. This value is very sensitive to the precision in the numerical integration due to the exponential function involved. For example, our numerical integrations with an accuracy of 1%, will give I with an uncertainty of around 5%. This is a rather good precision to test a model, but it is worth pointing out that, in general, the I-values obtained from stopping power calculations do not allow the determination of the mean excitation energy with the precision that clinical treatment of cancer patients would require [27, 28].

Our model predicts $I^{\rm SLPA}_{H_2O} = (73.5 \pm 3)$ eV. This value is close to the recommended value $I = 75$ eV in ICRU 49 (1993) [30] and to the theoretical values $I = 72$ eV [39] and $I = 73.2$ eV [40] obtained from the oscillator-strength spectrum. However, the average of I-values published in the last 20 years is higher, i.e. $I = (79.2 \pm 1.6)$ eV [79], with the experimental data generally above the theoretical values [42]. For example, recent measurements of the Bragg peak position [85] and range of ions in water (using the Bichsel rule [33]) agree with a mean excitation energy $I = (78.5 \pm 5)$ eV, close to the Bichsel *et al* [33] value $I = (79.7 \pm 5)$ eV. The accuracy is still far from what the medical applications require, but is lower than the 15% mentioned by Besemer *et al* [27].

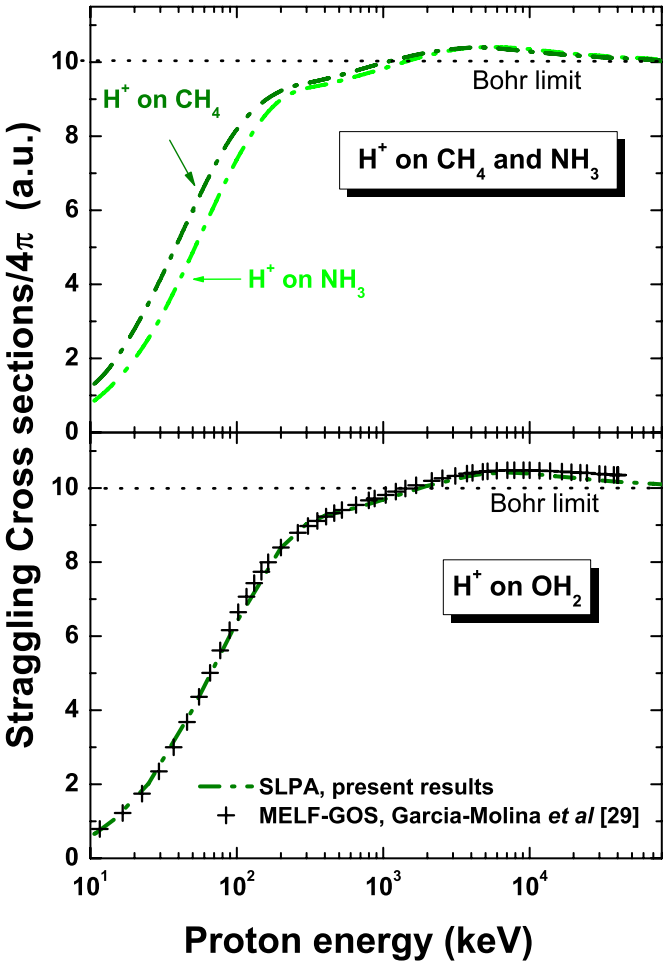

Figure 7. Straggling cross sections for CH_4 , NH_3 and H_2O. Curves: dot–dashed lines, present SLPA results. Symbols, MELF-GOS results by Garcia-Molina *et al* [29].

For the other molecular targets we obtained $I^{\rm SLPA}_{\rm CH_4} = (43 \pm 1)$ eV and $I^{\rm SLPA}_{\rm NH_3} = (57 \pm 2)$ eV, for methane and ammonia, respectively. Again the values are rather close to the recommended values $I_{\rm CH_4} = 41.7$ eV and $I_{\rm NH_3} = 53.7$ eV [86, 87], and to the theoretical values by Sauer *et al* [40] obtained from dipole oscillator strength distribution $I_{\rm CH_4} = 43.5$ eV and $I_{\rm NH_3} = 55.3$ eV.

3.6. Straggling

The second moment in the energy loss is known as energy-loss straggling. It represents the energy-loss variance per unit path length of a Gaussian energy-loss distribution [88]. Similar to the stopping power calculation, it must include all the electronic excited states. In the present contribution we deal with these calculations analogously to the stopping power ones, by using the SLPA including excitation and ionization.

At high energies, the straggling cross section per atom, Ω^2, tends to the known Bohr high-energy limit

$$\Omega^2_B = 4\pi Z^2_P N_e. \qquad (19)$$

In figure 7 we display the SLPA results for the straggling cross section over 4π. We display together the SLPA curves for CH_4 and NH_3 in the upper plot, while the values for water are shown in the bottom plot. In all the targets the tendency to the Bohr limit, i.e. $N_e = 10$, is clear, with a small shoulder above this value (4%) around (5–7) MeV. This shoulder is shifted with respect to the maximum of the stopping power, as binary collisional formalisms would expect [89, 90].

To our knowledge there are no experimental measurements in the literature for either of the molecules studied here. For water, we compare with the straggling results by the group of Abril and Garcia-Molina [29, 91, 92] using the semi-empirical MELF-GOS method. This method fits the experimental energy-loss spectrum in the optical range, and extends it to finite momentum transfers using Mermin-type dielectric function. The very deep shells are described using generalized oscillator strengths. The agreement is surprisingly good, which can be considered a good test for these two independent calculations.

4. Conclusions

The basic task of this article is to test the performance of our neonization method to deal with molecules composed by hydrides of the second row of the periodic table of elements. Our scheme is simple and computationally fast. We cover most of the inelastic magnitudes of experimental interest, proving that the method can describe the experiments with high reliability in the intermediate to high-energy region. We attribute the failure at lower energies to the theoretical approximations used. We expect our neonization scheme to hold even at lower impact energies with the use of an appropriate theoretical model.

The only two parameters in our calculations are the distance of the protons to the nucleus R, and the defect ε, which are displayed in the first two lines of table 1. Actually, it is possible to employ the *neonization* method eluding any Hartree–Fock calculation, just considering tables 2 (for SLPA) or 3 (for CDW–EIS) as starting points.

As already mentioned, the method is perfectly capable of being used to *neonizate* other molecules of biological interest such as OH^- and OH^+_3. Moreover, the extension of the present model to the *argonization* of the third row of the periodic table (molecules like SiH_4, PH_3, SH_2, and ClH) is in process.

Acknowledgments

This work was supported by the following Argentinian institutions: Consejo Nacional de Investigaciones Científicas y Técnicas (CONICET), Agencia Nacional de Promoción Científica, and Universidad de Buenos Aires.

References

[1] Moccia R 1964 *J. Chem. Phys.* **40** 2164
Moccia R 1964 *J. Chem. Phys.* **40** 2176
Moccia R 1964 *J. Chem. Phys.* **40** 2186
[2] Fainstein P D, Olivera G H and Rivarola R D 1996 *Nucl. Instrum. Methods Phys. Res.* B **107** 19
[3] Olivera G H, Fainstein P D and Rivarola R D 1996 *Phys. Med. Biol.* **41** 1633–47

[4] Nandi S, Biswas S, Khan A, Monti J M, Tachino C A, Rivarola R D, Misra D and Tribedi L C 2013 *Phys. Rev.* A **87** 052710

[5] Champion C, Galassi M E, Weck P F, Fojón O, Hanssen J and Rivarola R D 2012 Quantum-mechanical contributions to numerical simulations of charged particle transport at the DNA scale *Radiation Damage in Biomolecular Systems* ed G García Gómez-Tejedor and M Fuss (London: Springer) pp 263–90 chapter 16

[6] Champion C and Rivarola R D 2010 *Phys. Rev.* A **82** 042704

[7] Champion C 2010 *Phys. Med. Biol.* **55** 11–32

[8] Champion C and Dal Cappello C 2009 *Nucl. Instrum. Methods Phys. Res.* B **267** 881–4

[9] Boudrioua O, Champion C, Dal Cappello C and Popov Y V 2007 *Phys. Rev.* A **75** 022720

[10] Champion C, Boudrioua O and Dal Cappello C 2008 *J. Phys.: Conf. Ser.* **101** 012010

[11] Champion C 2003 *Phys. Med. Biol.* **48** 2147

[12] Rudd M E, Goffe T V, DuBois R D and Toburen L H 1985 *Phys. Rev.* A **31** 492

[13] Rudd M E, Itoh A and Goffe T V 1985 *Phys. Rev.* A **32** 2499

[14] Rudd M E, Kim Y-K, Madison D H and Gay Y J 1992 *Rev. Mod. Phys.* **64** 441

[15] Toburen L H and Wilson W E 1977 *J. Chem. Phys.* **66** 5202

[16] Bolorizadeh M A and Rudd M E 1986 *Phys. Rev.* A **33** 888
Bolorizadeh M A and Rudd M E 1986 *Phys. Rev.* A **33** 893

[17] Miller J H, Wilson W E, Manson S T and Rudd M E 1987 *J. Chem. Phys.* **86** 157

[18] Paul H 2013 Stopping power for light ions www.exphys.jku.at/stopping/

[19] Ziegler J F 2013 The stopping and range of ions in matter www.srim.org

[20] Shimizu M, Kaneda M, Hayakawa T, Tsuchida H and Itoh A 2009 *Nucl. Instrum. Methods Phys. Res.* B **267** 2667
Shimizu M, Kaneda M, Hayakawa T, Tsuchida H and Itoh A 2010 *Vacuum* **84** 1002

[21] Siiskonen T, Kettunen H, Peräjärvi K, Javanainen A, Rossi M, Trzaska W H, Turunen J and Virtanen A 2011 *Phys. Med. Biol.* **56** 2367–74

[22] Garcia-Molina R, Abril I, de Vera b P and Paul H 2013 *Nucl. Instrum. Methods Phys. Res.* B **299** 51–53

[23] Mitterschiffthaler C and Bauer P 1990 *Nucl. Instrum. Methods Phys. Res.* B **48** 58

[24] Phillips J A 1953 *Phys. Rev.* A **90** 532

[25] Baek W Y, Grosswendt B and Willems G 2006 *Radiat. Prot. Dosim.* **122** 32

[26] Reynolds H K, Dunbar F D N, Wenzel W A and Whaling W 1953 *Phys. Rev.* **92** 742

[27] Besemer A, Paganetti H and Bednarz B 2013 *Phys. Med. Biol.* **58** 887–902

[28] Paganetti H 2012 *Phys. Med. Biol.* **57** R99

[29] Garcia-Molina R, Abril I, Heredia-Avalos S, Kyriakou I and Emfietzoglou D 2011 *Phys. Med. Biol.* **56** 6475–93

[30] ICRU 1993 Stopping power and ranges for protons and alpha particles *ICRU Report* 49 (Bethesda, MD: ICRU)

[31] ICRU 2005 Stopping of ions heavier than helium *ICRU Report* 73 (Bethesda, MD: ICRU)
Also consider Sigmund P, Schinner A and Paul H 2009 Stopping of ions heavier than helium *ICRU Report* 73 (Bethesda, MD: ICRU) (errata and addenda)

[32] Bichsel H and Hiraoka T 1992 *Nucl. Instrum. Methods Phys. Res.* B **66** 345–51

[33] Bichsel H, Hiraoka T and Omata K 2000 *Radiat. Res.* **153** 208

[34] Krämer M, Jäkel O, Haberer T, Kraft G, Schardt D and Weber U 2000 *Phys. Med. Biol.* **45** 3299

[35] Emfietzoglou D, Pathak A, Papamichael G, Kostarelos K, Dhamodaran S, Sathish N and Moscovitch M 2006 *Nucl. Instrum. Methods Phys. Res.* B **242** 55

[36] Kumazaki Y, Akagi T, Yanou T, Suga D, Hishikawa Y and Teshima T 2007 *Radiat. Meas.* **42** 1683–91

[37] Dingfelder M, Hantke D, Inokuti M and Paretzke H G 1999 *Radiat. Phys. Chem.* **53** 1–18

[38] Garcia-Molina R, Abril I, Denton C D, Heredia-Avalos S, Kyriakou I and Emfietzoglou D 2009 *Nucl. Instrum. Methods Phys. Res.* B **267** 2647–52

[39] Kamakura S, Sakamoto N, Ogawa H, Tsuchida H and Inokuti M 2006 *J. Appl. Phys.* **100** 064905

[40] Sauer S P A, Sabin J R and Oddershede J 1995 *Nucl. Instrum. Methods Phys. Res.* B **100** 458–63

[41] Paul H, Geithner O and Jäkel O 2007 *Nucl. Instrum. Methods Phys. Res.* B **256** 561

[42] Sabin J R, Oddershede J and Sauer S P A 2013 On the determination of the mean excitation energy of water *Advances in Quantum Chemistry* ed Dz Belkic vol 65 (Amsterdam: Elsevier) pp 63–77

[43] Rudd M E, DuBois R D, Toburen L H, Ratcliffe C A and Goffe T V 1983 *Phys. Rev.* A **28** 3244–57

[44] Rudd M E, Kim Y-K, Madison D H and Gallagher J W 1985 *Rev. Mod. Phys.* **57** 965

[45] Lynch D J, Toburen L H and Wilson W E 1976 *J. Chem. Phys.* **64** 2616

[46] McNeal R J 1970 *J. Chem. Phys.* **53** 4308

[47] Wilson W E and Toburen L H 1975 *Phys. Rev.* A **11** 1303

[48] Wilson W E, Miller J H, Toburen L H and Manson S T 1984 *J. Chem. Phys.* **80** 5631

[49] Galassi M E, Rivarola R D, Beuve M, Olivera G H and Fainstein P D 2000 *Phys. Rev.* A **62** 022701

[50] Galassi M E, Abufager P N, Fainstein P D and Rivarola R D 2010 *Phys. Rev.* A **81** 062713

[51] Fernandez-Menchero L and Otranto S 2010 *Phys. Rev.* A **82** 022712

[52] Bourland P D, Chu K and Powers D 1971 *Phys. Rev.* B **3** 3625

[53] Bourland P D and Powers D 1971 *Phys. Rev.* B **3** 3635

[54] Fainstein P D, Ponce V H and Rivarola R D 1991 *J. Phys. B: At. Mol. Opt. Phys.* **24** 3091–119

[55] For a review on the SLPA see Montanari C C and Miraglia J E 2013 The dielectric formalism for inelastic processes in high energy ion-matter collisions *Advances in Quantum Chemistry* vol 65 ed Dz Belkic (Amsterdam: Elsevier) pp 165–201

[56] Levine Z H and Louie S G 1982 *Phys. Rev.* B **25** 6310

[57] Moskowitz W and Harrison M C 1965 *J. Chem. Phys.* **43** 3550

[58] Poet R 1978 *J. Phys. B: At. Mol. Phys.* **11** 3081

[59] Program nrhf.f at http://www3.nd.edu/~Johnson/Class01F/nrhf.f

[60] Clementi E (ed) 1990 *Modern Techniques in Computational Chemistry: MOTECC-90* (Leiden: ESCOM Science) p 111

[61] Zhan C-G, Nichols J A and Dixon D A 2003 *J. Phys. Chem.* A **107** 4184

[62] Gross E K U and Dreizler R M (ed) 1995 *Density functional Theory (NATO ASI Series)* (New York: Plenum)

[63] Becke A 1988 *Phys. Rev.* A **38** 3098

[64] Lee H, Lee Ch and Parr R G 1991 *Phys. Rev.* A **44** 768

[65] Montanari C C, Mitnik D M, Archubi C D and Miraglia J E 2009 *Phys. Rev.* A **80** 012901

[66] Cantero E D, Fadanelli R C, Montanari C C, Behar M, Eckardt J C, Lantschner G H, Miraglia J E and Arista N R 2009 *Phys. Rev.* A **79** 042904

[67] Montanari C C, Mitnik D M and Miraglia J E 2011 *Radiat. Eff. Defects Solids* **166** 338–45

[68] Montanari C C and Miraglia J E 2013 The energy loss straggling of low Z ions in solids and gases *AIP Conf. Proc.* **1525** 259–69

[69] Salvat F, Fernández-Varea J M and Williamson W Jr 1995 *Comput. Phys. Commun.* **90** 151

[70] Miraglia J E and Gravielle M S 2011 *Phys. Rev.* A **84** 062901

[71] Bethe 1930 *Ann. Phys.* **5** 325

[72] Werner U, Beckord K, Becker J and Lutz H O 1995 *Phys. Rev. Lett.* **74** 1962
[73] Gobet F, Farizon B, Farizon M, Gaillard M J, Carré M, Lezius M, Scheier P and Märk T D 2001 *Phys. Rev. Lett.* **86** 3751
[74] Luna H *et al* 2007 *Phys. Rev.* A **75** 042711
[75] Raot M V V S and Srivastava S K 1992 *J. Phys. B: At. Mol. Opt. Phys.* **25** 2175–87
[76] Itikawa Y and Mason N 2005 *J. Phys. Chem. Ref. Data* **34** 1
[77] Errea L F, Illescas C, Méndez L and Rabadán I 2013 *Phys. Rev.* A **87** 032709
[78] Bauer P, Käferböck W and Necas V 1994 *Nucl. Instrum. Methods Phys. Res.* B **93** 132
[79] Paul H 2013 On the accuracy of stopping power codes and ion ranges used for hadron therapy *Advances in Quantum Chemistry* vol 65 ed Dz Belkic (Amsterdam: Elsevier) pp 39–61
[80] Dagnac R, Blanc D and Molina D 1970 *J. Phys. B: At. Mol. Phys.* **3** 1239–51
[81] Toburen L H, Nakai M Y and Langley R A 1968 *Phys. Rev.* **171** 114
[82] Uehara S, Toburen L H, Wilson W E, Goodhead D T and Nikjoo H 2000 *Radiat. Phys. Chem.* **59** 1–11
[83] Francis Z, Incerti S, Karamitros M, Tran H N and Villagrasa C 2011 *Nucl. Instrum. Methods Phys. Res.* B **269** 2307–11
[84] Tschalar C and Bichsel H 1968 *Phys. Rev.* **175** 476
[85] Schardt D, Steidl P, Krämer M, Weber U, Parodi K and Brons S 2008 Precision Bragg-curve measurements for light-ion beams in water *GSI Scientific Report 2007* p 373
[86] Seltzer S M 1989 *NIST Electron and Positron Stopping Powers of Material Database, NIST Standard Reference Database 7* (Gaithersburg, MD: National Institute of Standards and Technology)
[87] ICRU 1984 Stopping powers for electrons and positions *ICRU Report* 37 (Bethesda, MD: ICRU)
[88] Besenbacher F, Andersen J U and Bonderup E 1980 *Nucl. Instrum. Methods* **168** 1
[89] Livingston M S and Bethe H A 1937 *Rev. Mod. Phys.* **9** 245–90
[90] Sigmund P and Schinner A 2003 *Eur. Phys. J.* D **23** 201
[91] Emfietzoglou D, Cucinotta F A and Nikjoo H 2005 *Radiat. Res.* **164** 202
[92] Garcia-Molina R, Abril I, Kyriakou I and Emfietzoglou D 2012 Energy loss of swift protons in liquid water: role of optical data input and extension algorithms *Radiation Damage in Biomolecular Systems* ed G García Gómez-Tejedor and M Fuss (London: Springer) pp 239–62 chapter 15